UDK 669.715:539.42
Original scientific article/Izvirni znanstveni članek

ISSN 1580-2949
MTAEC9, 42(5)191(2008)

# THE EFFECT OF COMPOSITIONAL VARIATIONS ON THE FRACTURE TOUGHNESS OF 7000 Al-ALLOYS

## VPLIV SPREMEMB V SESTAVI NA ŽILAVOST LOMA ALUMINIJEVE ZLITINE VRSTE 7000

**Maja Vratnica[1], Zorica Cvijović[2], Nenad Radović[2]**

[1] Faculty of Metallurgy and Technology, University of Montenegro, 81000 Podgorica, Cetinjski put b. b., Montenegro
[2] Faculty of Technology and Metallurgy, University of Belgrade, 11000 Belgrade, Karnegijeva 4, Serbia
majav@cg.ac.yu

*Prejem rokopisa – received: 2008-02-12; sprejem za objavo – accepted for publication: 2008-04-03*

To provide an understanding of how compositional variations affect the microstructural parameters associated with coarse intermetallic (IM) particles and the fracture toughness in AA 7000 aluminum forgings, a microstructural and fractographic analysis as well as mechanical tests were carried out on three industrially produced Al-Zn-Mg-Cu alloys with different contents of impurities (Fe+Si). Light optical microscopy and image analysis were used to assess the volume fraction, size and distribution of all the soluble and insoluble coarse (> 0.1 μm) IM particles identified in the corresponding R-C and L-R planes for T73-type heat treatments by selective etching and energy-dispersive X-ray spectroscopy. These quantitative data were correlated with the plain-strain fracture toughness, $K_{IC}$, with the results being used to produce useful information on alloy design and thermomechanical processing via microstructural control. The scanning electron microscope observation of fracture surface features and an estimation of the area fractions of different fracture modes in the plastic zone segments of a test specimen showed that multiple failure mechanisms occurred with coarse voiding at the intermetallics becoming more important as the fraction of coarse IM particles increases. A quantitative assessment of the relevant microstructural and fractographic parameters will be utilized for developing and verifying a multiple micromechanisms-based model for fracture toughness.

Key words : 7000 Al- alloys, chemical composition, microstructure, fracture toughness

S ciljem, da se ugotovi, kako spremembe v sestavi vplivajo na parametre mikrostrukture, odvisne od velikih delcev intermetalnih spojin (IM), in na žilavost loma v izkovkih iz zlitine AA 7000, so bile izvršene mikrostrukturne, mikrofraktografske in mehanske preiskave pri treh industrijskih zlitinah Al-Zn-Mg-Cu z različno vsebnostjo nečistoč (Fe + Si). Optična mikroskopija in analiza slike sta bili uporabljeni za določitev volumenskega deleža, velikosti in porazdelitve topnih in netopnih velikih (>0,1 μm) IM-zrn v ustreznih R-C- in L-R-ploskvah po toplotni obdelavi T73 s selektivnim jedkanjem in z disperzivno spektroskopijo rentgenskih žarkov. Ti kvantititivni podatki so bili korelirani z žilavostjo loma $K_{IC}$, dobljeni pa so bili tudi podatki, ki so koristna informacija za načrtovanje zlitin in termomehansko obdelavo s kontrolo mikrostrukture. Analiza prelomnih površin z vrstičnim mikroskopom in določitev površine različnih deležev preloma v plastični zoni preizkušancev je pokazala več vrst mehanizmov preloma in nastanek tem več velikih jamic ob IM-zrnih, čim večji je bil delež teh velikih zrn. Kvantitativna ocena relevantnih mikrostrukturnih in mikrofraktografskih parametrov bo uporabljena za razvoj in za verifikacijo modela žilavosti loma na podlagi več mahanizmov preloma.

Ključne besede: aluminijeva 7000 zlitina, kemična sestava, mikrostruktura, žilavost loma

## 1 INTRODUCTION

High-strength aluminum alloys of the AA 7000 (Al-Zn-Mg-Cu) series are widely used for structural applications due to their good combination of specific strength and fracture toughness[1]. However, the critical fracture toughness properties, especially in the short transverse direction, may be seen as questionable, since the fracture resistance is influenced by a number of parameters, including a range of microstructural features that are controlled by the chemistry and processing[1,2,3,4]. Furthermore, the microstructural anisotropy associated with wrought materials may influence the failure mode depending on the load and crack orientation[2].

It is now recognized that the coarse particles of intermetallic (IM) phases are generally detrimental to the fracture properties. This is associated with the fact that although the fracture processes in precipitation-hardened AA 7000 alloy products involve multiple micromechanisms, the decohesion and fracture of these particles, which are brittle and have weak interface bonding, is the first step in a sequence of events that lead to the overall material fracture[1,2,5]. The remaining fracture path is partitioned between intergranular fracture and micro-void-induced transgranular fracture.

The undesirable coarse particles with sizes in the range of 1 μm to 20 μm are IM phases of two types: (a) insoluble Fe- and Si-bearing phases formed during the solidification process, and (b) normally soluble phases containing alloying elements that do not completely dissolve during the homogenization and solution treatment[1]. In order to improve the toughness, it is necessary to achieve the lowest levels of coarse IM particles. The removal of excess amounts of the soluble particles is possible by controlling all the stages of processing. But, the limits on the reduction of the Fe and Si impurities are set by the cost and the availability of high-purity materials. Consequently, these impurities are always present in commercial alloys. They react with Al and alloying elements such as Mg and Cu to form a large

number of phases[6]. In addition, these alloys contain Mn and Cr, which may also be present in the form of coarse IM particles, since they combine with Fe, Si and Al.

Therefore, it is of interest to predict the variation in the fracture properties as a function of the microstructural parameters, such as the volume fraction of coarse IM particles, their size and their spatial distribution. However, most of the available information is concerned with the properties of wrought alloys. Systematic and in-depth quantitative microstructural and fractographic examinations of commercial AA 7000 alloys in the form of thick plates cut out from forgings have not been widely conducted. It is the purpose of this contribution to report on a microstructural and fractographic investigation of the effect of compositional variations on the attributes associated with coarse IM particles and the fracture toughness of modern AA 7000 alloy forgings (the high-zinc variant) in the over-aged condition as a function of test orientation. The failure mechanisms are identified and the individual contributions to the overall fracture are quantitatively assessed. The data are then used to obtain a relationship between the microstructural parameters and the plane-strain fracture toughness, with the results being utilized for the modeling of toughness.

## 2 EXPERIMENTAL

Three industrial alloys with Zn, Mg, and Cu levels broadly in the range of the AA 7049 composition were received in the form of hot-forged ≈50-mm-thick pancake-type plates. The chemical composition of each alloy is given in **Table 1**. The amounts of alloying elements are very near to the nominal ones. The only difference in composition between the alloys is the total (Fe+Si) content, which increases gradually from alloy 1 through alloy 3. **Figure 1** shows the cutting of the tests specimens from the received plates.

All three alloys were solution treated at 460 °C for 1 h, water-quenched, and aged to a T73 temper. The two-step T73 over-aged treatment consisted of the aging of the specimens for 5 h at 100 °C and 5 h at 160 °C. Light optical microscopy (LOM) and image analyses were used to characterize the microstructure of the as-heat-treated plates. Metallographic sections were taken from the corresponding R-C and L-R planes. The specimens were then prepared using standard metallographic techniques. A selective etching and energy-dispersive X-ray spectroscopy (EDS) analysis on a scanning electron microscope (SEM) were used to identify the IM phases present. The volume fraction of all the soluble and insoluble coarse IM particles, $V_V$, their size expressed by the average intercept length, $L$, and the mean free path, $\lambda$, characterizing the space distribution were assessed with the line-intercept method. The measurements were carried out on 500 uniformly sampled microstructural frames at a magnification of 1000 times. Plane-strain fracture-toughness tests were performed in accordance with ASTM E399 on the specimens of the corresponding R-C and L-R orientations, i.e., on the single-edge-notched three-point bending specimens (SEB) of R-C orientation and the compact-tension (CT) specimens of L-R orientation. The specimens were fatigue pre-cracked according to the ASTM standard specifications. In all cases, three specimens were tested. The $K_{IC}$ values for the R-C orientation specimens were obtained from the $J$-integral data. $J_{IC}$ was evaluated with the unloading compliance technique, with a single specimen for each $J_{IC}$ result. The $J$-integral and the crack growth, $\Delta a$, were calculated in accordance with ASTM E1152 and ASTM E813. On a broken specimen an SEM fractographic examination was performed to explain the fracture mechanism. The fracture surface morphology was investigated in the central region of the plastic zone ahead of the fatigue pre-crack. The area fraction of the microvoid-induced transgranular fracture regions, $A_{At}$, the intergranular fracture regions, $A_{Ai}$, and the coarse IM particles, $A_{Ap}$, were estimated. The area measurements were performed on SEM fractographs by tracing the areas on a digitizing

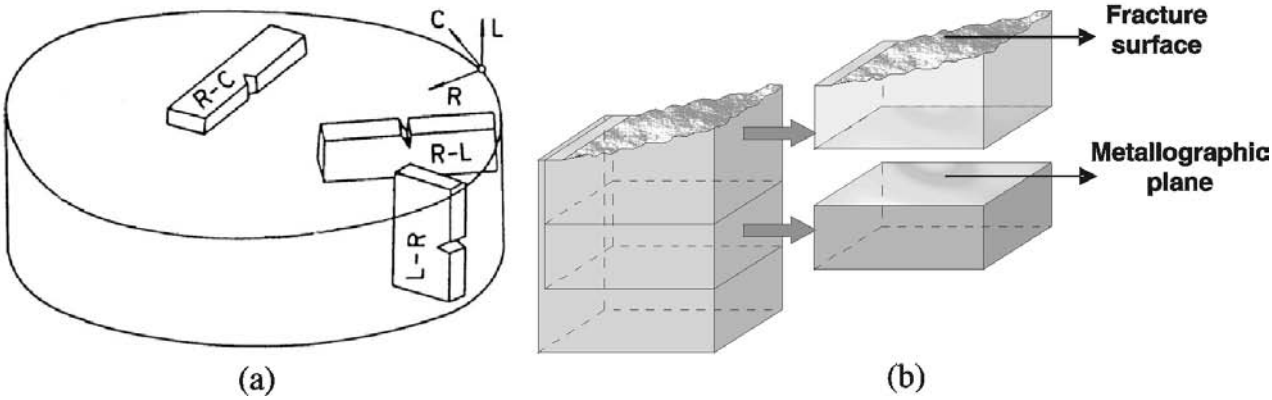


**Figure 1:** (a) Schematic illustration of the specimen orientations used for the fracture-toughness tests (L-longitudinal direction, C-circumferential or tangential direction, R-radial direction) and (b) locations of the metallographic planes for the microstructural analysis (b)
**Slika 1:** (a) Shema orientacije vzorcev, uporabljenih za preizkuse žilavosti loma (L-vzolžna smer, C tangencialna smer, R – radialna smer) in (b) mesto odvzema vorcev za mikrostrukturno analizo

tablet. These measurements provided the data to quantify the contributions of the different fracture micromechanisms to the plane-strain fracture-initiation process as a function of the purity degree and the specimen orientation.

## 3 RESULTS AND DISCUSSION

### *3.1 Analysis of the microstructural data*

Typical microstructures of simple uniaxially forged material after the full heat treatment are illustrated in **Figure 2**.

All the forgings show a deformed dendrite cell structure with coarse IM particles having an average size of 1.27–2.43 μm. As expected, relatively coarse and closely spaced precipitates, mostly situated on the grain boundary surrounded by the precipitate-free zones (PFZs), were also observed (**Figure 2a**). The TEM characterization of the precipitation in AA 7000 alloys by previous authors[1,2] indicates that these particles are variants of the $\eta$-$Mg(Cu,Al,Zn)_2$ phase. In the Al-rich matrix there was a dense population of uniformly distributed dispersoids[1,2,4] and fine precipitates of the $\eta$ and $\eta'$ phases[1,2] that contributed to the precipitation hardening. On the other hand, the coarse IM particles are inhomogeneously distributed and aligned in the direction of the prevailing deformation, as observed on the metallographic plane of L-R orientation (**Figure 2b**). The micrographs also illustrate the IM particles that are irregularly shaped and of different types (**Figures 2c and d**). The combined use of the metallographic and EDS analyses indicates that these particles are of the following types: (a) soluble $Mg(Cu,Al,Zn)_2$, S-$CuMgAl_2$, and, most often observed, $Mg_2Si$, (b) the Fe-bearing phases $Al_7Cu_2Fe$, $(Cu,Fe,Mn)Al_3$ and a very little of $(Cu,Fe,Mn)Al_6$, (c) the Cr-bearing phase $(Cu,Fe,Mn,Cr)Al_7$, and (d) another type of Si-containing phases $(Fe,Cr,Mn,Cu)_3SiAl_{12}$.

The identified phases were found in all three alloys; however, variations in the composition caused large changes in their fraction and their morphological characteristics. This observation was also supported by the image analyses. As can be seen from the data presented in **Table 2**, the alloy 3 had the highest percentage of

**Table 1:** Chemical composition of the investigated alloys (in mass fractions, *w*/%)
**Tabela 1:** Kemična sestava raziskanih zlitin (v masnih deležih, *w*/%)

| Alloy | Elements | | | | | | | | | | |
|---|---|---|---|---|---|---|---|---|---|---|---|
| | Zn | Mg | Cu | Mn | Cr | Zr | Ti | V | B | Fe | Si |
| 1 | 7.45 | 2.47 | 1.53 | 0.25 | 0.17 | 0.15 | 0.015 | 0.003 | 0.003 | 0.12 | 0.11 |
| 2 | 7.30 | 2.26 | 1.55 | 0.29 | 0.18 | 0.13 | 0.015 | 0.007 | 0.003 | 0.16 | 0.09 |
| 3 | 7.65 | 2.26 | 1.55 | 0.25 | 0.18 | 0.11 | 0.017 | 0.005 | 0.003 | 0.26 | 0.11 |

**Table 2:** Results of the image analysis and the plane-strain fracture-toughness tests
**Tabela 2:** Razultati analize slike in določitve žilavosti loma

| Alloy | Plane | $K_{IC}$/(MPa·m$^{1/2}$) | $A_A$* | | IM phase characteristics | | | |
|---|---|---|---|---|---|---|---|---|
| | | | | | Type | $V_V$, $\varphi$/% | $L$/μm | λ/μm |
| 1 | R-C | 45.50 | ND*** | | $MgZn_2$+S | 0.159 | 1.63 | 1024.8 |
| | | | | | Fe-rich** | 0.227 | 2.00 | 883.5 |
| | | | | | $Mg_2Si$ | 0.125 | 1.74 | 1394.1 |
| | L-R | 43.16 | P | 0.152 | $MgZn_2$+S | 0.147 | 1.56 | 1054.7 |
| | | | I | 0.278 | Fe-rich** | 0.236 | 2.08 | 878.0 |
| | | | T | 0.570 | $Mg_2Si$ | 0.144 | 1.94 | 1350.0 |
| 2 | R-C | 42.63 | ND*** | | $MgZn_2$+S | 0.048 | 1.29 | 2685.6 |
| | | | | | Fe-rich** | 0.357 | 1.99 | 557.0 |
| | | | | | $Mg_2Si$ | 0.094 | 1.70 | 1806.7 |
| | L-R | 40.96 | P | 0.299 | $MgZn_2$+S | 0.095 | 1.27 | 1333.8 |
| | | | I | 0.304 | Fe-rich** | 0.440 | 2.06 | 465.5 |
| | | | T | 0.397 | $Mg_2Si$ | 0.134 | 1.92 | 1425.1 |
| 3 | R-C | 40.53 | ND*** | | $MgZn_2$+S | 0.119 | 1.63 | 1363.4 |
| | | | | | Fe-rich** | 0.590 | 2.43 | 409.8 |
| | | | | | $Mg_2Si$ | 0.147 | 1.95 | 1318.7 |
| | L-R | 37.67 | P | 0.378 | $MgZn_2$+S | 0.046 | 1.38 | 3031.4 |
| | | | I | 0.287 | Fe-rich** | 0.532 | 2.37 | 444.3 |
| | | | T | 0.335 | $Mg_2Si$ | 0.146 | 2.09 | 1434.8 |

* Area fractions of microvoid-induced transgranular fracture regions (t), intergranular fracture region (i), and coarse constituent particles (p); ** Fe-rich phases = $Al_7Cu_2Fe$ + $(Cu,Fe,Mn)Al_3$ + $(Cu,Fe,Mn)Al_6$ + $(Cu,Fe,Mn,Cr)Al_7$ + $(Fe,Cr,Mn,Cu)_3SiAl_{12}$ ; *** ND = not determined
* delež površine mikrojamičastega transkristalnega preloma (t), interkristalen prelom (i) in velikih IM- zrn (p); ** Z Fe bogate faze = $Al_7Cu_2Fe$ + $(Cu,Fe,Mn)Al_3$ + $(Cu,Fe,Mn)Al_6$ + $(Cu,Fe,Mn,Cr)Al_7$ + $(Fe,Cr,Mn,Cu)_3SiAl_{12}$ ; *** ND = ni določeno

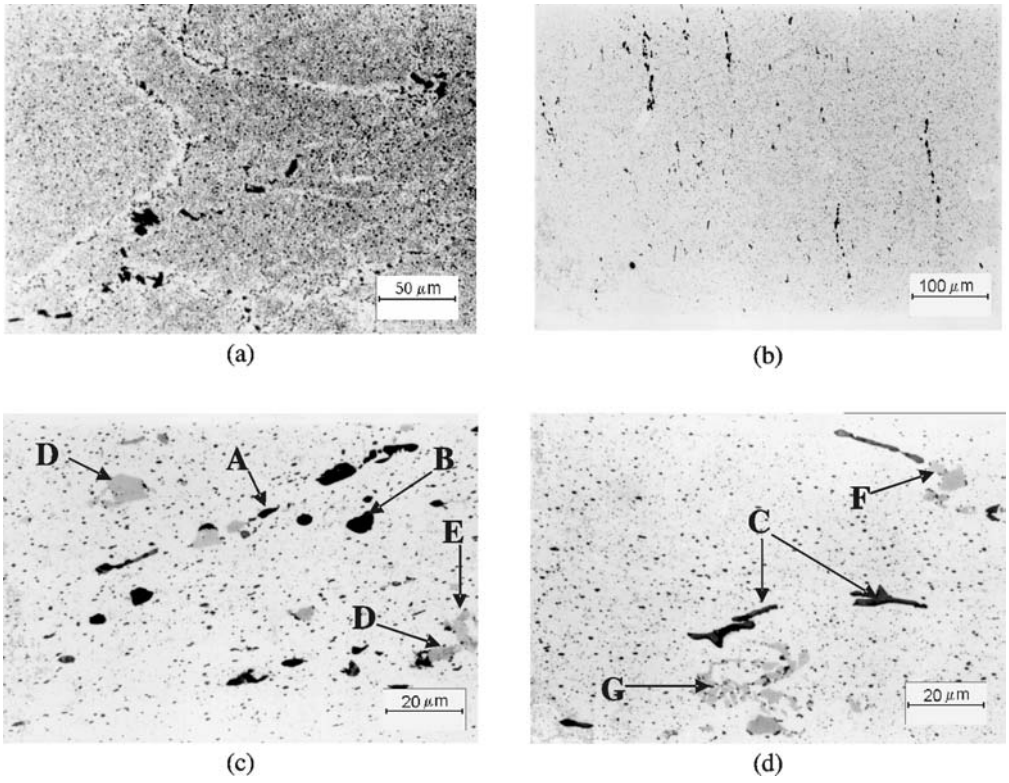


**Figure 2:** Optical microstructures of the over-aged alloy 3 (a),(c),(d) and alloy 1 (b) observed in R-C (a),(c) and L-R planes (b),(d) etched in 10 % $H_3PO_4$ at 50 °C for 5 min (a) and Keller's reagent at 20 °C for 5 s (b), (c), (d). Type of phases: A = $Mg(Cu,Al,Zn)_2$, B = S-$CuMgAl_2$, C = $Mg_2Si$, D = $(Cu,Fe,Mn)Al_3$ or $(Cu,Fe,Mn)Al_6$, E = $Al_7Cu_2Fe$, F = $(Cu,Fe,Mn,Cr)Al_7$, G = $(Fe,Cr,Mn,Cu)_3SiAl_{12}$.

**Slika 2:** Optična slika prestarane zlitine 3 (a), (b), (c) in (d) in zlitine 1 (b) v ploskvah R-C (a) in (c) ter L-R v ploskvah (b) in (d), jedkano v 10 % $HPO_4$ 5 min (a) in s Keller reagentom 5 s pri 20 °C (b), (c) in (d). Vrste faz: A – $Mg(Cu,Al,Zn)_2$, B – S-$CuMgAl_2$, C – $Mg_2Si$, D – $(Cu,Fe,Mn)Al_3$ ali$(Cu, Fe,Mn)$ $Al_6$, E – $Al_7Cu_2Fe$, F – $Cu,Fe,Mn,Cr)Al_7$, G – $Fe,Cr,Mn,Cu)_3SiAl_{12}$

coarse particles, with an average of volume fraction of 0.79 %, while the alloys 1 and 2 had a similar volume fraction, varying between about 0.52 % and 0.58 %. The significant increase in the amount of coarse particles, serving as the crack-initiation sites, is a direct consequence of an increase in the total (Fe+Si) content. For all the alloys, i.e., the volume fraction of phases containing Al, Mg, Cu, and Zn ($Mg(Cu,Al,Zn)_2$ and S-$CuMgAl_2$) is lower than $\approx$ 0.15 %. Note also that, since the Si content is practically unchanged from one alloy to the other, the volume fraction of $Mg_2Si$ particles is constant. This implies that the Fe content plays an important role in the formation of coarse particles. The volume fraction of grey particles (Fe-containing phases) increases almost linearly with the increase in the Fe content. As a result, the coarse particles are distributed over shorter distances. These features can provide planes of easy crack growth, thereby reducing the deformation capacity of the matrix.

### *3.2 Toughness behavior*

**Table 2** shows how reducing the total (Fe+Si) content and thereby removing most of the coarse IM particles improves $K_{IC}$. As expected, the toughness was the highest for the alloy 1, with the lowest (Fe+Si) content of the mass fraction ($w$) 0.23 %. By increasing the impurity level from 0.23 % to 0.25 % and in turn the volume fraction of the Fe- and Si-containing particles from the volume fraction ($\varphi$) 0.380 % to 0.574 %, the $K_{IC}$ value in the R-C orientation decreased by approximately by 6.5 %. Since in alloy 2 the Si content is $w$ = 0.02 % and lower than that in the alloy 1, it is concluded that large variations in the amount of coarse particles and the fracture toughness can occur with a relatively small change in the Fe content. The toughness decreased further when going to a purity of $w$ = 0.37 %. The drop in the fracture toughness, due to the presence of undesirable particles – $\varphi$ = 0.298 % greater than in the microstructure of alloy 1 – is almost of 11 %.

The trend is similar for the L-R orientation. Although the amount of damaged particles has the greatest influence, a more probable explanation for the toughness degradation found in this work may be based on the synergistic effect of the coarse particles' volume fraction, their sizes and spacing. Namely, as the (Fe+Si) content increases the particle size increases, while the mean free path decreases, with a concomitant decrease in toughness. Thus, although the average particle size vary between 1.70 μm and 2.08 μm for the alloys 1 and 2, no distinct variation of the Fe-containing particle size with the orientation of the metallographic plane were

observed, whereas for the alloy 3 the particle size seemed to vary from 1.95 μm to 2.43 μm, with only minor differences between the R-C and L-R orientation planes. It should be noted that the Fe-containing particles were larger than those of the $Mg_2Si$ phase and hence, more detrimental to $K_{IC}$, although a contribution from the other phases particles cannot be ruled out. Namely, larger particles are cracked more often. Also, the particles aligned in the loading direction are more prone to this type of damage. Therefore, the distribution of coarse particles is of particular importance. The metallographic examination showed that the spacing of the weak paths is also affected (at least for the R-C orientation plane). Decreasing the amount of particles leads to an increase in the mean interparticle distances. The $\lambda$ value increases by 60 % to 80 %, going from alloy 3 to alloy 1, causing the absence of most particle stringers and decreasing the extent of coarse voiding with the IM particles. The comparison of the R-C and L-R orientations indicates that for a given degree of purity, the fracture toughness is different for a different direction of testing. All three alloys showed a higher toughness for the R-C-orientation specimens, as compared to that for the L-R orientation. This toughness anisotropy is particularly notable for alloy 3, with the highest (Fe+Si) content. The $K_{IC}$ value in the R-C direction is higher by 7 % than the short-transverse value. This is primarily attributed to the anisotropic orientations of the coarse IM particles. This is consistent with the previously reported results[1,5] and indicates that the alignment of these particles seriously reduces $K_{IC}$ and that it is even more efficient than the other possible paths of weakness, e.g., the grain boundaries with stringers of precipitates. Since coarse particles are brittle and fracture or separate from the matrix when the local strain exceeds a critical value, they provide preferential crack paths ahead of a crack at a high stress intensity. When such a stress intensity is applied, the presence of these preferential crack paths decreases the energy needed for the crack propagation. Hence, the toughness degradation can be attributed to an acceleration of the crack initiation and growth by the damaged particles.

The relative contributions of the different fracture modes to the plain-strain fracture initiation process (and, therefore, to $K_{IC}$) were determined from the fracture surfaces of the failed toughness specimens. SEM observations of the fracture surfaces revealed the multimechanism of the fracture process as a competition between coarse voiding at the IM particles and transgranular/intergranular failure. The controlling mechanism varies with the alloy purity, with the combination of transgranular/intergranular shearing dominating in alloy 1 (**Figure 3a**), and the coarse voiding becoming progressively more important as the (Fe+Si) content increases (**Figure 3b**).

The transgranular microvoid-induced fracture generated with the formation of voids around the matrix precipitates was observed in all cases. The shear planes

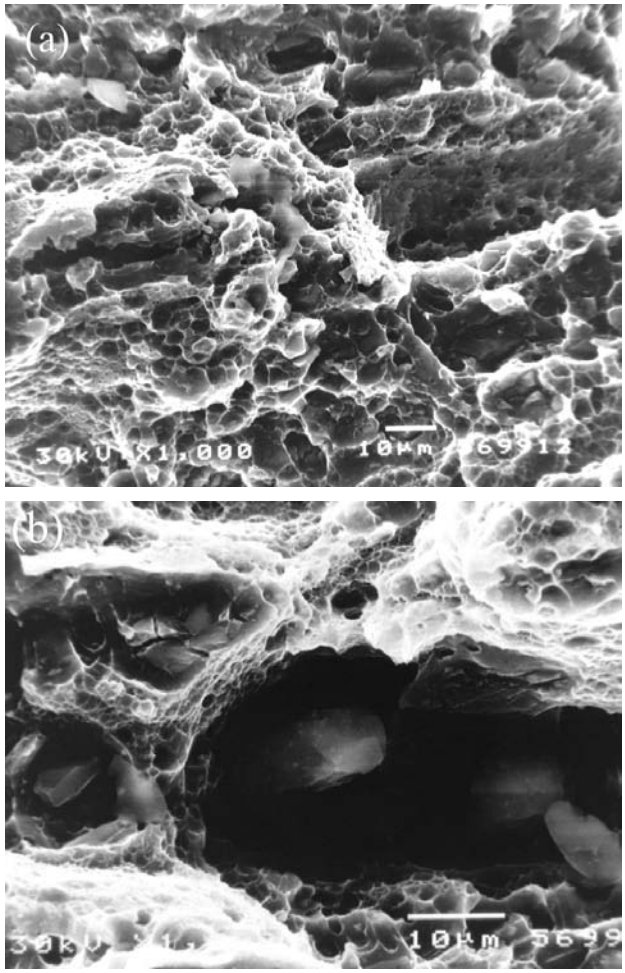


**Figure 3:** SEM micrographs showing the R-C fracture plane of alloy 1 (a) and the L-R fracture plane of alloy 3 (b).
**Slika 3:** SEM-posnetek preloma v R-C-ploskvi pri zlitini 1 (a) in L-R-preloma zlitine 3 (b)

were covered with fine dimples, commonly associated with very fine particles. Many extremely fine dimples, representing areas of extensive deformation that preceded the ductile fracture, were observed on the walls of very large dimples associated with the aggregates of mostly fractured IM particles. Places called ridges, where the crack had changed its direction of propagation, could also be identified. A higher magnification examination showed that they appear to be formed on the grain boundaries. Flat intergranular areas were characterized by a fine population of shallow dimples and coarse grain-boundary precipitates on some of them. The presence of the ridges suggests a competition between intergranular and transgranular shear-fracture mechanisms, although a greater extent of grain-boundary failure has not been observed.

In spite of the general similarity of the fracture surfaces for the alloy 1 through alloy 3, significant differences were also observed. The crack-propagation modes and the toughness levels are dependent on the extent of the primary void growth prior to the outset of

the secondary failure mode (i.e., intergranular and transgranular shear crack growth) and the intervoids linking. Since the primary voids initiate at coarse IM particles, it may be expected that an increase in the (Fe+Si) level, which in turn increases the amount of these particles, leads to an increased number of fractured particles, and therefore, a smaller extent of intergranular/transgranular shear fracture. **Figure 2b** illustrates this point very clearly, and it is also confirmed by the quantitative data in **Table 2**. The area fraction, $A_{At}$, of the microvoid-induced transgranular fracture decreases systematically with an increase in the volume fraction of the Fe- and Si-containing particles, while the area fraction, $A_{Ap}$, of the coarse IM particles on the fracture surface increases, leading to a decrease in the fracture toughness.

## 4 CONCLUSIONS

Quantitative microstructural and fractographical data showed that the coarse Fe- and S-containing particles had a very detrimental effect on the fracture toughness of over-aged Al-Zn-Mg-Cu forgings. The drop in $K_{IC}$ was consistent with a change in the dominant failure mechanism, from intergranular/transgranular shear to extensive coarse void growth as the (Fe+Si) content increases from $w$ = 0.23 to 0.37 %. This effect was attributed to the amount, size and spatial arrangement of the coarse IM particles and demonstrates the orientation dependence of the fracture toughness and the morphological anisotropy of the microstructure.

## 5 REFERENCES

[1] N. U. Deshpande, A. M. Gokhale, D. K. Denzer, John Liu, Metallurgical Materials Transactions A, 29A (**1998**) 4, 1191

[2] B. Morere, J.-C. Ehrstrom, P. J. Gregson, I. Sinclar, Metallurgical Materials Transactions A, 31A (**2000**) 10, 2503

[3] N. Kamp, I. Sinclair, M. J. Starink, Metallurgical Materials Transactions A, 33A (**2002**) 4, 1125

[4] R. C. Dorward, D. J. Beerntseen, Metallurgical Materials Transactions A, 26A (**1995**) 9, 2481

[5] A. M. Gokhale, N. U. Deshpande, D. K. Denzer, J. Liu, Metallurgical Materials Transactions A, 29A (**1998**) 4, 1203

[6] L. F. Mondolfo, Aluminium alloys, Structure and Properties, Butterworts, London 1976